Available online at www.sciencedirect.com
ScienceDirect
Journal of Catalysis 249 (2007) 67–78
JOURNAL OF CATALYSIS
www.elsevier.com/locate/jcat

Temperature-dependent N_2O decomposition over Fe-ZSM-5: Identification of sites with different activity

E. Berrier [a], O. Ovsitser [a], E.V. Kondratenko [a], M. Schwidder [b], W. Grünert [b], A. Brückner [a,*]

[a] *Leibniz-Institut für Katalyse an der Universität Rostock e.V., Branch Berlin (former ACA), P.O. Box 96 11 56, D-12474 Berlin, Germany*
[b] *Lehrstuhl für Technische Chemie, Ruhr-Universität Bochum, D-44780 Bochum, Germany*

Received 9 January 2007; revised 22 March 2007; accepted 25 March 2007

Abstract

Decomposition of N_2O has been studied in the temperature range $293 < T < 673$ K over Fe-ZSM-5 with 0.3 wt% extra-framework Fe after prereduction in H_2/Ar or Ar flow at $473 < T < 973$ K. Two different processes of reoxidation of reduced Fe^{2+} species by N_2O were identified: (i) a fast one starting at ≈500 K involving deposition of atomic oxygen on isolated Fe^{2+} species, leading to the formation of $Fe^{3+}O^{\bullet-}$ sites detected by EPR spectroscopy (site 1), and (ii) a slow one related mainly to the reoxidation of small Fe_xO_y clusters (site 2), the formation of which cannot be avoided in H_2/Ar flow. The number of sites 1 increases with rising prereduction temperature, whereas sites 2 are independent of T_{red}. $O^{\bullet-}$ formation could not be detected on reoxidation of Fe species by O_2. For the first time, a direct relation between Fe^{2+} reoxidation by N_2O and formation of $O^{\bullet-}$ could be detected by EPR spectroscopy, suggesting that the so-called "α-oxygen" first described by Panov et al. is an $O^{\bullet-}$ radical anion. Based on in situ XANES experiments, this makes it highly unlikely that the previously discussed ferryl moiety (Fe^{4+}=O) is the source of the highly active oxygen.

Keywords: Fe-ZSM-5; N_2O decomposition; Active sites; XANES; UV–vis-DRS; EPR

1. Introduction

Iron-modified MFI catalysts have attracted much attention in recent years because of their promising efficiency in a wide range of reactions of environmental and industrial interest, including selective catalytic reduction (SCR) of NO_x by ammonia and hydrocarbons [1–3], selective oxidation of benzene to phenol [4–7], oxidative dehydrogenation of propane to propene [8], and direct decomposition and SCR of N_2O [9,10]. Since the pioneering work of Panov et al. [4], who discovered first the unique ability of so-called "O_α" formed on contact of Fe-ZSM-5 with N_2O to selectively oxidize benzene to phenol at room temperature, debate has been ongoing about the nature of such iron–oxygen species, particularly with respect to their nuclearity and charge. Panov et al. [11] suggested that this type of atomic oxygen can be formed only on reduced binuclear Fe sites, even in samples with an Fe content as low as 0.056 wt% [12]:

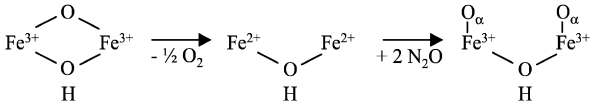

(1)

Beyond the nuclearity of Fe species inside the MFI pore network, the form in which N_2O deposits its oxygen on these Fe sites is also controversial. After initially disregarding the formation of $O^{\bullet-}$ anion radicals, Panov and co-workers [13] later became convinced that O_α is just this type of species. They based this conclusion on a comparison of the amount of Fe with the amount of oxygen deposited below 523 K, which led to a ratio of $O_{dep}/Fe \approx 1$ [12,13]. Considering a change of the Fe valence state from +2 to +3 [Eq. (1)], it seems plausible to attribute the aforementioned unique activity of Fe-ZSM-5 to Fe^{3+}–$O^{\bullet-}$ sites, although no direct experimental evidence has been given.

In an earlier study on N_2O decomposition at 623 K over different Fe-ZSM-5 catalysts (1.4 and 5.0 wt% Fe) by in situ EPR

* Corresponding author. Fax: +49 30 6392 4454.
E-mail address: brueckner@aca-berlin.de (A. Brückner).

0021-9517/$ – see front matter
doi:10.1016/j.jcat.2007.03.027

spectroscopy, we were able to detect a strong radical signal as soon as the samples (prereduced with CO at the same temperature) came in contact with N_2O [14]. We assigned this signal to $O^{\cdot-}$. However, at the reaction temperature of 623 K, simultaneous desorption of O_2 must be taken into account. Thus, the possibility that this O_2 reacts with reduced Fe^{2+} to form $O_2^{\cdot-}$ cannot be ruled out; this may also contribute to the radical signal observed. Moreover, the experimental conditions in our previous study differed markedly from those of Panov et al. insofar as this radical signal was observed on samples with a rather high Fe content (1.4 and 5.0 wt%, respectively).

Alternatively, Kiwi-Minsker et al. [15] suggested $Fe^{4+}{=}O$ as active species formed on N_2O decomposition over a reduced binuclear Fe site at 523 K. But these authors did not provide any experimental evidence for this species. Their conclusion was based on DFT calculations of the terminal Fe–O bond length of such hypothetical Fe sites [16]. They also found that only at the lowest Fe concentration (200 ppm) all Fe sites were active in the uptake of oxygen, leading to a ratio of $O_{dep}/Fe \approx 1$, whereas for the higher Fe content (1000 ppm), only about 25% of all Fe sites were found to be active [17].

The formation of $Fe^{4+}{=}O$ ferryl groups on decomposition of N_2O over Fe-ZSM-5 was also suggested by Sachtler and coworkers [18] on the basis of their in situ XANES and EXAFS results. They attributed the increased intensity of the XANES pre-edge peak after N_2O treatment to a change from octahedral to tetrahedral Fe coordination and assumed that the latter was tetravalent. Moreover, they assigned a Fe–O distance of 0.181 nm in the EXAFS spectrum to $Fe^{4+}{=}O$. Both conclusions are not unambiguous, because it is very well known that Fe^{3+} also can be tetrahedrally coordinated, and the distance of 0.181 nm for a Fe=O double bond seems too long compared with the value of 0.161 nm derived from DFT calculations [16].

Very recently, Pirngruber et al. [19] performed in situ resonant inelastic X-ray scattering (RIXS) measurements of N_2O decomposition at 533 K over 0.1–0.4 wt% Fe-ZSM-5 pretreated in He at 870–1170 K. Despite observing a marked reaction of N_2O with a major fraction of the Fe sites, they could not detect the K_β satellite line in the pre-edge region of the absorption spectrum, which, however, was clearly visible in a Fe^{4+}-containing reference sample. From this, they concluded that the species formed by Eq. (1) does not contain a $Fe^{4+}{=}O$ ferryl group but does contain a $Fe^{3+}{-}O^{\cdot-}$ group.

In summary, there is no doubt that a special, highly reactive oxygen species is created on low-temperature decomposition of N_2O over Fe-MFI catalysts with extra-framework Fe sites pretreated either in reductive or inert atmosphere or in vacuum to create reduced Fe species. This works for a wide range of Fe concentrations, from values as low as 200 ppm [16] up to about 5 wt% [14,19]. By TPR experiments it was found that this particular kind of oxygen gives rise to a sharp peak at much lower temperature than seen for conventional oxide ions [15,19]. Interestingly, a similar result was also obtained over Fe-ferrierite, suggesting that the ability to create highly effective oxygen from N_2O may not be restricted to the MFI structure [20]. One reason for the lack of commonly accepted knowledge on the nature of this particular Fe–O site is probably the fact that it was mostly identified indirectly by reaction with various gaseous reactants, not directly by a spectroscopic technique. Moreover, little is known about the behavior of the Fe sites during pretreatment, uptake, and release of this oxygen. Therefore, we have studied Fe-ZSM-5 with the major percentage of Fe sites being located in extra-framework single sites by a combination of different in situ techniques that can detect both changes of the Fe valence state and coordination (UV–vis, EPR, XAS) as well as radicals that may be formed from oxygen species (EPR). Moreover, we used a pulse technique operating at ambient pressure with mass spectrometric detection to quantify the number of oxygen atoms deposited from N_2O per Fe ion. Through integrative evaluation of all of these results, we intended to identify the nature of the "magic" oxygen species formed from N_2O in contrast to reaction with O_2 and thus provide an answer to this still-controversial question.

2. Experimental

The catalyst studied was prepared by improved liquid ion exchange as described in detail previously [1]. In brief, a commercial Na-ZSM-5 (Si:Al = 14) and Fe powder (Goodfellow "carbonyl iron") were stirred in 0.1 m HCl under a protective gas atmosphere for 5 days, washed with deionized water (separating residual iron with a magnet), dried, and calcined in air at 873 K for 2 h. The Fe content of the sample as determined by ICP-OES was 0.3 wt%. The residual Na content was insignificant; no other ions were introduced on purpose. The preparation procedure did not change the micropore volume of the zeolite, which was 0.15 $cm^3\,g^{-1}$ before and 0.13 $cm^3\,g^{-1}$ after Fe introduction.

XANES spectra at the Fe*K*-edge (7112 keV) were measured at Hasylab beamline E4 (Hamburg, Germany) using a Si(111) double-crystal monochromator. The absorption spectra were measured in transmission mode in an in situ cell described elsewhere [21]. An iron metal foil was measured at the same time (between the second and third ionization chambers) for energy calibration. Data were treated using the XANES Dactyloscope for Windows software [22]. Spectra were recorded after oxidation of the sample at 873 K (1 h in flowing dry air), after reduction at temperatures between 773 and 873 K (1 h in 20% H_2/N_2 or H_2/He, with temperatures the limits for the heating element in the gas mixtures used), and after reoxidation in 2% N_2O/N_2 at different temperatures. For this purpose, the sample was heated in the N_2O-containing mixture to the desired temperature (5 $K\,min^{-1}$), kept there for 10 min, and cooled to room temperature for acquisition of the spectrum. Measurements at the reoxidation temperature were not performed regularly because of a slight temperature dependence of the spectrum shortly after the edge, which would have impaired quantitative analysis.

In situ UV/vis-DRS measurements were performed with a Cary 400 spectrometer (Varian) equipped with a diffuse reflectance accessory (Praying Mantis, Harrick) and a heatable reaction chamber (Harrick). Fe-ZSM-5 was diluted by α-Al_2O_3 in a ratio of 1:3 to reduce light absorption. For comparison, the parent Na-ZSM-5 was measured under the same conditions.

However, its contribution to the total spectral intensity of the Fe-ZSM-5 was negligible. The samples were used as powders and placed in a 5-mm-diameter, 3-mm-deep sample cup, at the bottom of which is a small sieve. The temperature was controlled by a thermocouple located on the bottom of the sample cup, connected to a temperature controller (Eurotherm). Reactant gases were provided by mass flow controllers (Bronkhorst) and led from top to bottom through the sample layer. Spectra were converted in Kubelka–Munck functions and in certain cases were deconvoluted in Gaussian subbands using the GRAMS/32 program (Galactic). For analyzing the N_2O decomposition kinetics, the diluted sample was prereduced at different temperatures (673, 773, or 873 K) in a flow of 20% H_2/Ar (20 ml min^{-1}) for 1 h, cooled to 523 K in Ar flow and exposed to a flow of 2% N_2O/He (20 ml min^{-1}) at 523 K. Kinetic parameters of reoxidation of reduced iron species by N_2O were obtained by monitoring the absorbance at a certain wavelength as a function of time and fitting the received curves by a pseudo-first-order rate law assuming two different sites,

$$C_{ox} = C^0_{red1}\left[\exp(-k_1 \cdot t)\right] + C^0_{red2}\left[\exp(-k_2 \cdot t)\right]. \quad (2)$$

Here C_{ox} is the total number of sites being reoxidized during treatment in N_2O flow, C^0_{red1} and C^0_{red2} are the initial numbers of reduced iron sites when starting the reoxidation after reductive pretreatment, and k_1 and k_2 are the apparent first-order rate constants of reoxidation.

In situ EPR spectra in X-band ($\nu \approx 9.5$ GHz) were recorded with a cw-spectrometer ELEXSYS 500-10/12 (Bruker) using microwave power of 6.3 mW, modulation frequency of 100 kHz, and modulation amplitude of 0.5 mT. The magnetic field was measured with respect to the standard 2,2-diphenyl-1-picrylhydrazyl hydrate (DPPH). A homemade quartz plug–flow reactor connected to a gas-dosing system containing mass flow controllers (Bronkhorst) was implemented in the rectangular cavity of the spectrometer. All in situ experiments used 50 mg of catalyst particles 125–200 μm in diameter. A special EPR cell consisting of two concentric tubes, with the inner tube connected to the gas inlet, was used to detect oxygen radical species that may form on deposition of O from N_2O at 523 K. The sample was placed between the inner and outer tubes to ensure proper gas through-flow. After 2 h of pretreatment in Ar flow at 973 K, the sample was cooled to 523 K and the gas flow was switched to 2% N_2O/He flow for 30 min. Then it was rapidly quenched to 77 K, and the EPR spectrum was recorded at this temperature.

To relate the amount of decomposed N_2O to the number of Fe sites in the sample, N_2O decomposition was also studied by pulse experiments at ambient pressure using a catalytic plug–flow reactor connected to a quadrupol mass spectrometer and gas mixtures of 10% N_2O/Ne (3.4 μmol N_2O per pulse) and 5% N_2O/Ne (1.7 μmol N_2O per pulse), respectively. The catalyst (0.1 g) was charged inside the isothermal zone of the reactor without dilution with inert particles. Before pulsing N_2O, the catalyst was prereduced in a 5% H_2/N_2 flow (40 ml min^{-1} [STP]) at 673, 773, 873, or 973 K (10 K min^{-1}) for ca. 30 min, followed by cooling to 523 K in the same flow. Hereafter, the H_2 flow was replaced by Ne flow, to remove hydrogen. Then a N_2O/Ne mixture was pulsed at 523 K. Alternatively, the catalyst was pretreated in H_2 flow at 873 K and cooled to 423, 473, or 523 K, at which point N_2O pulse experiments were performed. To check whether oxygen deposited on N_2O decomposition at 523 K desorbs slowly at this temperature, the catalyst was kept in Ne flow at the same temperature for 30 min after saturation with deposited oxygen, after which another series of N_2O pulses was performed. The feed components and reaction products were analyzed using a quadruple mass spectrometer (Balzer Omnistar). The following atomic mass units (AMUs) were monitored: 44 (N_2O), 32 (O_2), 30 (N_2O), 28 (N_2O, N_2), 20 (Ne), 18 (H_2O), and 2 (H_2). The concentrations of feed components and reaction products were determined from the respective AMUs using standard fragmentation patterns and sensitivity factors.

3. Results and discussion

3.1. Characterization of the sample in the initial and the reduced states

The UV–vis spectrum of the hydrated as-received Fe-ZSM-5 catalyst is characterized by broad, partially overlapping $Fe^{3+} \leftarrow O$ charge transfer (CT) bands (Fig. 1a, thick black line). To discriminate between different Fe species, the experi-

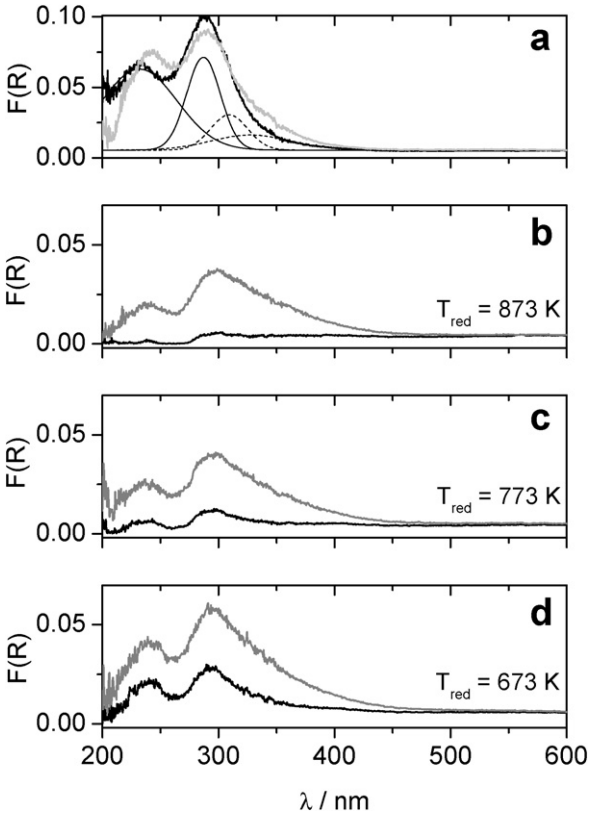

Fig. 1. (a) UV–vis-DR spectra measured at 293 K of Fe-ZSM-5 in as-received hydrated form (black thick line) including deconvoluted sub-bands (black thin lines) and in dehydrated form after calcination in O_2 flow at 823 K (grey thick line); (b–d) UV–vis-DR spectra measured at 523 K after 1 h reduction in 20% H_2/Ar at the denoted temperature (black) and after 20 min exposure to 2% N_2O/He flow at 523 K (grey line).

mental spectrum is deconvoluted into several subbands, the assignment of which has been discussed in detail previously [23,24] and is based on earlier proposals [25,26]. Briefly, subbands below 250 nm arise from isolated Fe^{3+} sites in tetrahedral coordination, whereas those in higher coordination (5 or 6 oxygen ligands) show an additional band around 290 nm besides the one below 250 nm. Subbands at 300–400 and above 400 nm are assigned to oligomeric FeO_x clusters and large Fe_2O_3 particles, respectively. Based on the position and the area of the deconvoluted subbands in Fig. 1a, it can be concluded that the catalyst contains about 90% of the total Fe content in the form of isolated Fe^{3+} species in both tetrahedral and higher coordination along with a small amount of small oligonuclear clusters, as reflected by the dashed subbands. After heating in air to 823 K (Fig. 1a, thick grey line) the CT band at 288 nm decreases in favor of the band at 242 nm. This suggests that some higher-coordinated Fe^{3+} single sites become tetrahedral by loosing H_2O ligands from their coordination sphere. Moreover, absorbance around 350 nm increases slightly, suggesting that the thermal treatment leads to partial agglomeration of isolated Fe^{3+} sites to oligonuclear Fe_xO_y clusters, an effect that has been reported previously [23].

Fig. 2 gives the Fe*K* XANES spectra for the calcined state and after two reduction runs (810 and 840 K) and compares them with spectra of reference compounds. After calcination at 873 K, the presence of Fe^{3+} in the sample is obvious. The intensity rises in the same energy range as with α-Fe_2O_3, although the edge energies determined from the first inflection point are

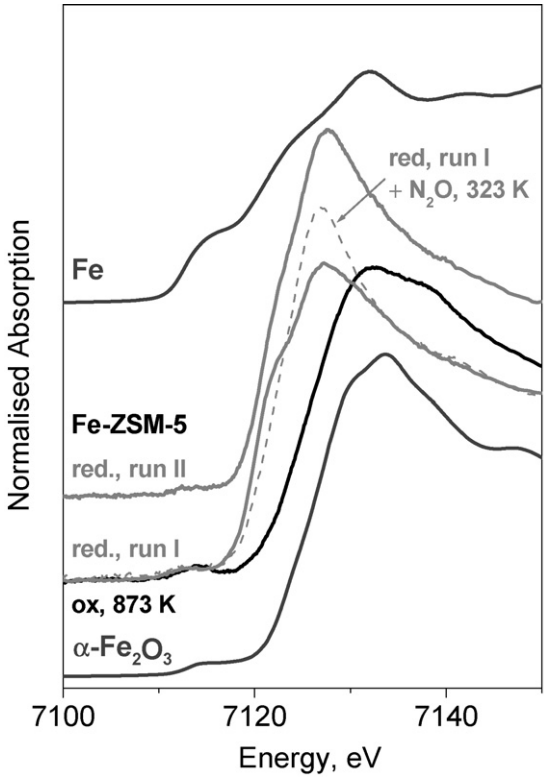

Fig. 2. Fe*K* XANES of Fe-ZSM-5 after calcination in O_2 flow at 823 K, after reduction in 20% H_2/He at 810 K (run I) or 840 K (run II) and after interaction of the catalyst reduced at 810 K (run I) with 2% N_2O/N_2 at 323 K.

different due to subtle deviations in the edge shape. In the reduction runs, a strong edge shift was generated, but the spectra were not identical, with a more pronounced shoulder and consequently a larger shift for run I with the lower reduction temperature. When the reduction product of run I was exposed to flowing N_2O/N_2 at 323 K, the low-temperature shoulder disappeared completely.

In the literature, edge shifts found between Fe in +3 and +2 oxidation states differ strongly due to differing edge shapes and experimental resolution. In earlier studies, average shifts of 2.4 eV were reported [27], whereas spectra of similar shape and quality as shown in Fig. 2 resulted in 3.7–3.8 eV edge shifts between Fe_2O_3 and FeO or $FeSiO_4$ [28,29]. In our case, the difference is >4 eV even after low-temperature N_2O treatment of the reduced sample (oxidized: 7125.4 eV; red. run I + N_2O: 7121.2 eV).

For the reduction product of run I, the large shift, the shoulder, and a nonzero pre-edge intensity may suggest the presence of some metallic iron. A priori, reduction to Fe^0 cannot be excluded because the sample contains a minor amount of small oligonuclear Fe_xO_y clusters (Fig. 1a) for which TPR studies suggested that such reduction to zerovalent Fe may occur at around 800 K [30–32]. Interaction of the reduction product of run I with N_2O at 323 K quenches the low-energy shoulder and shifts the absorption edge to higher energy. If this change were caused by reoxidation of Fe^0, then it should be possible to reproduce the experimental spectrum after reduction run I by a linear combination of the spectrum after adsorption of N_2O at 323 K and that of a Fe metal foil (Fig. 2). This attempt was not successful, however. Thus, it is very likely that edge shift and shoulder after reduction run I arise not from Fe^0, but rather from asymmetries in the coordination sphere around Fe^{2+} (deviation from centrosymmetry), which increases transition probabilities to near-edge d states from the Fe*K* level. Adsorption of N_2O removes the asymmetry and its consequences in the spectrum. The spectrum obtained after this treatment permits rejecting Fe(0) even in small quantities. Thus, even if minor quantities of Fe metal were formed during catalyst reduction, they would be reoxidized by N_2O (and indicated by N_2 release) at very low temperatures. In reduction run II, adsorption of trace oxygen impurities may have caused the low intensity of the low-energy shoulder at the absorption edge.

The sensitivity of the reduction process to oxygen traces and to the flow conditions (relevant for water removal) is also reflected in the UV–vis-DR spectra (Figs. 1b–1d) and in the EPR spectra (Fig. 3). The strong decay of the $Fe^{3+} \leftarrow O$ CT bands with increasing reduction temperature is obvious; however, even at 873 K, there is still significant intensity in the 288 nm region, whereas earlier TPR work [13,29] and the XANES spectra in Fig. 2 rather suggest that Fe^{3+} should be completely reduced at this temperature. Residual Fe^{3+} was also detected by EPR after autoreduction in Ar at 973 K (Fig. 3c); reduction in 20% H_2/Ar at 873 K was even less effective.

Fig. 3 also shows the EPR spectrum of the initial sample in hydrated form. Signals at effective g values of $g' \approx 6.3, 4.3$, and 2 can be seen, which are known from earlier studies [1,14,23,33]. Based on their behavior during dehydration/rehydration ex-

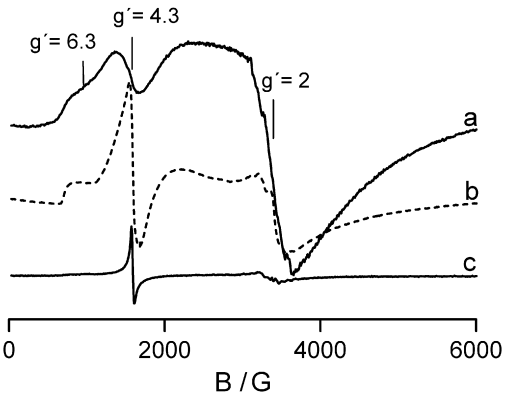

Fig. 3. EPR spectra of the hydrated as-received Fe-ZSM-5 measured at 293 K (a) and 77 K (b) and EPR spectrum of the same sample after 1.5 h treatment at 973 K in Ar flow measured at 77 K (c).

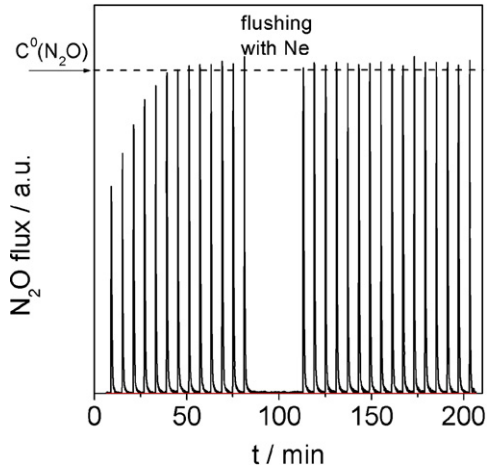

Fig. 4. N_2O concentration measured at the reactor outlet after pulsing N_2O at 523 K over Fe-ZSM-5 prereduced in 5% H_2/N_2 flow at 873 K.

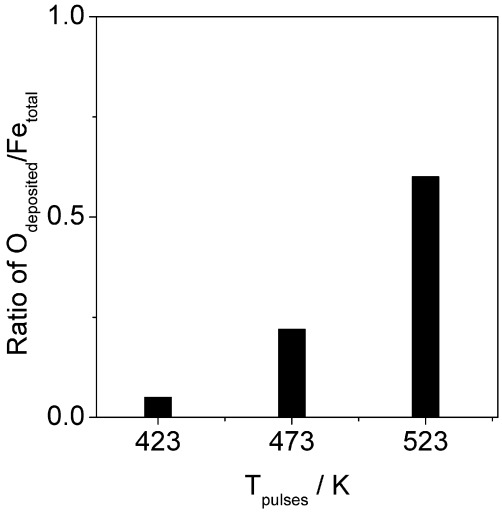

(a)

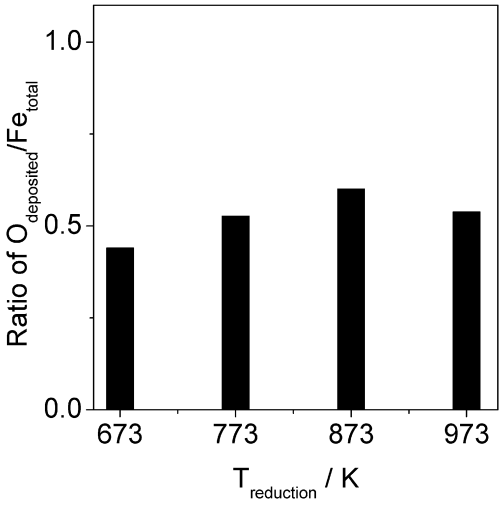

(b)

Fig. 5. Number of oxygen atoms deposited per Fe site in Fe-ZSM-5: (a) as a function of temperature after reductive pretreatment at 873 K and (b) at 523 K as a function of pretreatment temperature.

periments [23], the $g' \approx 4.3$ and 6.3 signals have been assigned to isolated Fe^{3+} species in strongly distorted tetrahedral and higher coordination, respectively. The $g' \approx 2$ line can arise from different sources. In samples containing only isolated Fe^{3+}, it was attributed to sites of high symmetry, for which a discrimination between tetrahedral and higher coordination is not possible. However, Fe_xO_y clusters, reflected by UV–vis bands above 300 nm (Fig. 1a), also contribute to the $g' \approx 2$ signal [1, 23]. This is particularly evident from the temperature dependence of this line, which decreases on cooling to 77 K, due to antiferromagnetic interactions between neighboring Fe^{3+} sites within clusters (Fig. 3, a and b). In contrast, the signal intensity of highly symmetric isolated Fe^{3+} sites should be inversely proportional to the temperature due to the Curie–Weiss law. Because the intensity of the $g' \approx 2$ signal in Fig. 3 decreases on cooling to 77 K, it is considered to arise mainly from Fe_xO_y clusters.

3.2. Oxygen deposition from N_2O studied by pulse experiments

Typical N_2O transient responses on pulses of 10% N_2O/Ne at 523 K after pretreatment in a flow of 5% H_2/N_2 at 873 K are plotted in Fig. 4. The N_2O concentration detected at the reactor outlet increases with the number of N_2O pulses and reaches a constant value after seven N_2O pulses, corresponding to the inlet concentration of the gas mixture. This indicates that the oxygen defect sites created by the reductive pretreatment are saturated by oxygen deposition from N_2O. No gas-phase O_2 could be detected, demonstrating that recombination of deposited atomic O species and desorption as O_2 does not occur at 523 K. Another important observation from Fig. 4 is the fact that no further N_2O decomposition was observed after flushing the catalyst with Ne for 30 min at 523 K. This suggests that the deposited O species are stable under these conditions, because they cannot be removed in Ne flow to regenerate active sites for N_2O decomposition.

Fig. 5 relates the number of deposited O species (calculated from these pulse experiments) to the total number of Fe sites at different temperatures of reoxidation (Fig. 5a) or prereduction (Fig. 5b). For a given reduction temperature of 873 K, the amount of deposited O species increases gradually with the re-

oxidation temperature (Fig. 5a). This suggests that Fe sites of different activity may be involved in N_2O decomposition. When the prereduction temperature is raised from 673 to 873 K, the O/Fe ratio obtained after N_2O decomposition at 523 K increases slightly, but decreases surprisingly again after pretreatment at 973 K (Fig. 5b). In any case, the O/Fe ratio remains close to 0.5. If the sample was dominated by Fe_xO_y oligomers, this result would be plausible by assuming that N_2O deposits its oxygen into an oxygen vacancy between two reduced Fe^{2+} sites, whereby each of these transfers one electron to generate two Fe^{3+} and one O^{2-}. However, the Fe-ZSM-5 used in this study is clearly dominated by isolated Fe sites (Fig. 1a), for which such a process is not possible. This raises the questions of which and how many Fe sites are involved in the uptake of O deposited by N_2O. Consequently, we performed in situ UV–vis and EPR studies because these techniques can directly monitor the redox behavior of coexisting Fe sites.

3.3. Temperature-dependent N_2O decomposition studied by in situ UV–vis-DRS and EPR

Fig. 6 illustrates the temporal evolution of the UV–vis absorbance bands at 234 and 290 nm (i.e., the maximum CT bands of isolated Fe^{3+} in tetrahedral and higher coordination) on reoxidation of reduced FeO_x species in N_2O/He flow at different temperatures. All absorbance profiles show a similar qualitative evolution: Below 480 K, no significant change is observed. Between 480 and 550 K, a steep increase reflects reoxidation of

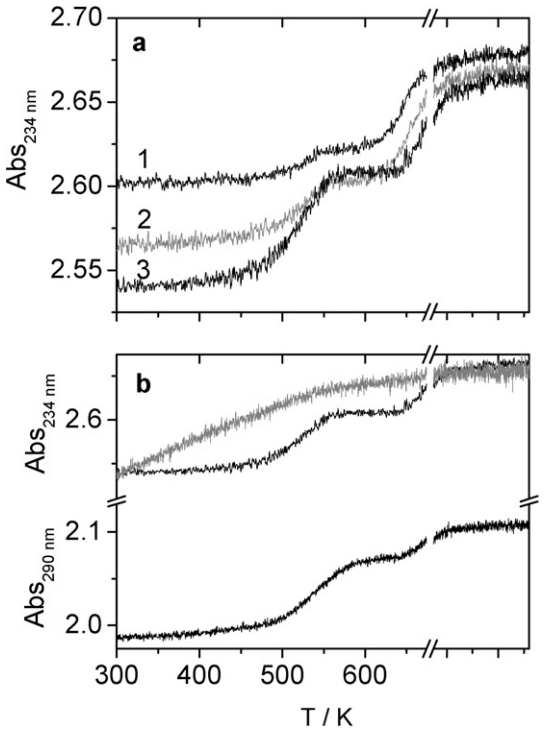

Fig. 6. Evolution of absorbance during heating in 2% N_2O/He flow to 673 K with 10 K min^{-1} followed by a 10 min isothermal hold: (a) at 234 nm after reduction at 673 K (1), 773 K (2) and 873 K (3), (b) at 234 and 290 nm after reduction at 873 K. For comparison, reoxidation in pure O_2 flow is also shown in (b), grey line.

Fe^{2+} to Fe^{3+}, followed by an apparent steady state before reoxidation of the remaining Fe^{2+} sites in a second step between 650 and 673 K, fully restoring the absorbance values measured before reduction. The temperature range of the first step at $T < 550$ K agrees well with previous results of Kiwi-Minsker et al. [17] and also with the results of pulse experiments described above (Fig. 4), in which N_2 evolution but no O_2 evolution could be detected at 523 K.

The UV–vis experiments in Figs. 1b–1d show definitively that oxygen deposition from N_2O at 523 K is connected with reoxidation of some of the Fe^{2+} sites. The increasing absorbance is completely caused by oxidation of Fe^{2+}; any Fe^0 formed on severe reduction would have been reoxidized already at ≈300 K (see above). The temperature of the reductive pretreatment has a strong effect on the starting absorbance level (residual Fe^{3+} after reduction, Figs. 1b–1d) and on the amplitude of the low-temperature (LT) step (Fig. 6). Only a small number of Fe^{2+} sites able to catalyze N_2O decomposition below 550 K is formed after prereduction at 673 K, whereas approximately half of the Fe sites participate in this step after reduction at 873 K (Figs. 1b, 1d, and 6a). In the transient pulse experiments the ratio between oxygen deposited from N_2O at 523 K and the total number of Fe sites, O_{dep}/Fe_{total}, was found to be close to 0.5 (Fig. 5). Taking into account that only half of the total Fe sites can be reoxidized by oxygen from N_2O below 550 K after reduction at 873 K (Fig. 5a), the O_{dep}/Fe_{active} ratio would be close to 1. This suggests that (i) each active Fe^{2+} takes up one O, as proposed previously [12,13,17,20] and (ii) not all Fe^{2+} species in the sample can provide this low-temperature activity, and more such species are formed at higher pretreatment temperatures. The first statement, which is seemingly straightforward, contradicts well-substantiated conclusions from transient kinetic studies by Kondratenko and Pérez-Ramírez [34,35]. We discuss this problem below.

As mentioned above, the steady state observed above 550 K (Fig. 6) is only an apparent one. The course of Fe^{2+} reoxidation by N_2O in this range depends critically on the heating rate. The plateau observed at 10 K min^{-1} (Fig. 6) is absent at 4 K min^{-1}, but at 20 K min^{-1}, the Fe^{3+} concentration decreases temporarily (not shown). This suggests that Fe^{2+} reoxidation by N_2O is superimposed by a faster process above 550 K—namely, autoreduction of Fe^{3+} to Fe^{2+} by liberation of O_2—an effect that also was observed by other authors above 600 K [12,17]. The higher the reduction temperature, the longer the plateau, suggesting that the amount of active Fe–O sites capable to act as precursors for O_2 formation and desorption is clearly linked to the temperature of prereduction. Moreover, the absorbance curves decrease immediately when switching from N_2O/He to Ar flow after reaching the plateau at 550 K (Fig. 7).

In contrast, admission of O_2 onto the N_2O-treated catalyst at the same temperature causes immediate oxidation of all iron, suggesting that O_2 is much more active than N_2O. Thus, it is probable that the high-temperature (HT) reoxidation step above 650 K may be governed not only by N_2O decomposition, but also by readsorption and reaction of the O_2 liberated above 550 K.

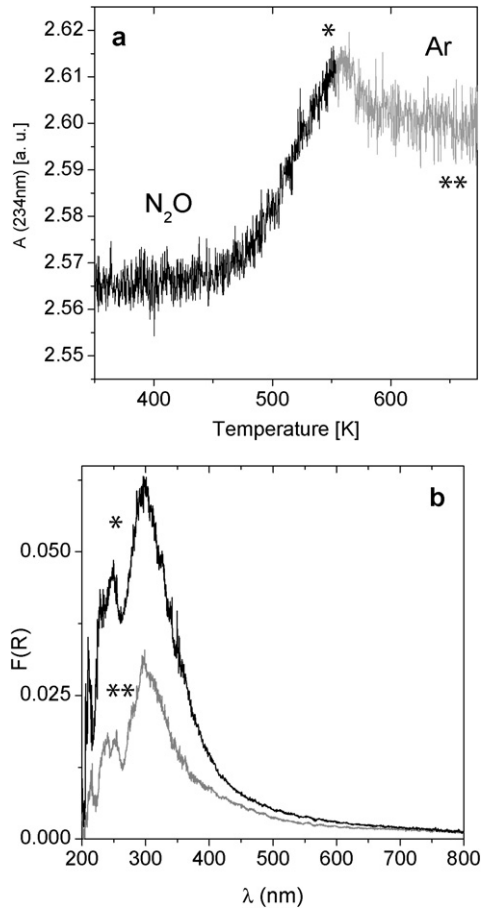

Fig. 7. Evolution of absorbance during heating with 10 K min^{-1} in N_2O/He flow to 550 K and further in Ar flow (a) and corresponding UV–vis spectra (b).

Interestingly, different step heights in Fig. 6 suggest that the number of Fe^{2+} reoxidized in the LT step strongly increases with the pretreatment temperature, whereas the HT step height seems to be independent of the pretreatment, at least when the latter exceeds 673 K. This points to the fact that at least two different kinds of Fe species might exist in the catalyst, one that is easily reducible but hardly reoxidizable by N_2O and one showing the opposite behavior. These differences are not seen when O_2 is used instead of N_2O; in that case, gradually faster reoxidation of all reduced Fe sites occurs from the very beginning (Fig. 6b).

A similar temperature-dependent study was performed by in situ EPR spectroscopy. Fig. 8 depicts EPR spectra recorded during stepwise heating in N_2O flow from Fe-ZSM-5 prereduced at 873 K. At a temperature matching exactly that of the first step in the UV absorbance curves (Fig. 6), three signals appear arising from Fe^{3+} in tetrahedral ($g' \approx 4.3$) and higher coordination ($g' \approx 6.4$ and 5.6). It is also evident from Fig. 8 that a broad line at $g' \approx 2$ gains intensity as well, most likely due to the reoxidation of oligomeric clusters that might have been formed during the reductive pretreatment. All of these results are in very good agreement with the aforementioned observations in UV–vis spectroscopy and indicate that all three types of Fe species (tetrahedral- and higher-coordinated single sites, as well as small clusters) are able to abstract and retain atomic oxygen from N_2O at 523 K without evolution of O_2. Interestingly, the low-field signals of isolated Fe^{3+} appear suddenly above 473 K and do not grow any further above 573 K, whereas the line at $g' \approx 2$ rises gradually throughout the entire temperature range. This suggests that the activity towards N_2O decomposition varies among Fe sites. The sites giving rise to the low-field signals may be reoxidized in an activated, fast process, whereas a slow process is responsible for the reoxidation of the species related to the $g' \approx 2$ signal.

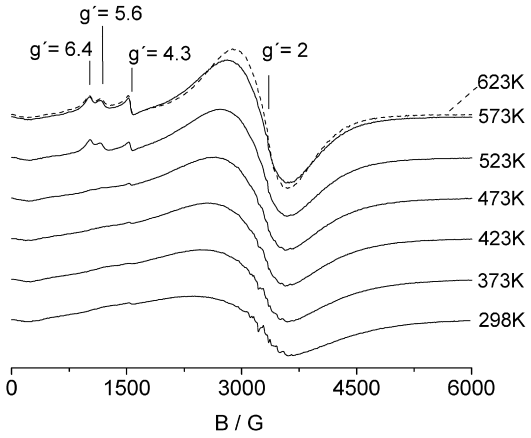

Fig. 8. In situ EPR spectra measured during heating in 2% N_2O/He after reduction in H_2/Ar at 873 K.

Wichterlová and co-workers identified three different sites for isolated metal ions in ZSM-5: in the straight channels (α), in the intersection between the straight and sinusoidal channels (β) and in a boat shape site in the sinusoidal channel (γ) [36]. Although this information was originally derived for Co^{2+} ions from UV–vis data, it has been analogously adopted for Fe ions [37]. Cu and Co ions are most easily reduced when located in α positions; reduction is not as easy in β and γ positions [38]. It has not explicitly been stated whether the same is true for Fe ions. However, assuming that this is the case, it would mean that the low-field EPR signals should arise from Fe^{3+} sites in β ($g' \approx 6.4$ and 5.6) and γ sites ($g' \approx 4.3$), whereas the $g' \approx 2$ line might comprise isolated sites in α sites as well as small clusters in the main channels of the ZSM-5 structure. The increasing distortion ($\alpha < \beta < \gamma$) reflected by the position of the EPR signals also would agree with confinement of the Fe^{3+} sites in the respective pore position, which is most restricted in the boat-shaped γ site [23]. Higher site distortion is one possible cause of higher reactivity. To explore the reactivities of the different Fe sites in more detail, isothermal $Fe^{2+} \rightarrow Fe^{3+}$ reoxidation kinetics after different pretreatments were followed by UV–vis-DRS, as described in the next section.

3.4. Kinetics of isothermal Fe reoxidation studied by UV–vis-DRS

The evolution of absorbance at 290 and 234 nm was monitored during treatment in N_2O/He flow at 473 and 523 K after prereduction of Fe-ZSM-5 in H_2/Ar flow at 673 and 873 K, respectively. As an example, the kinetic curves obtained at 290 nm together with the fits using a first-order rate

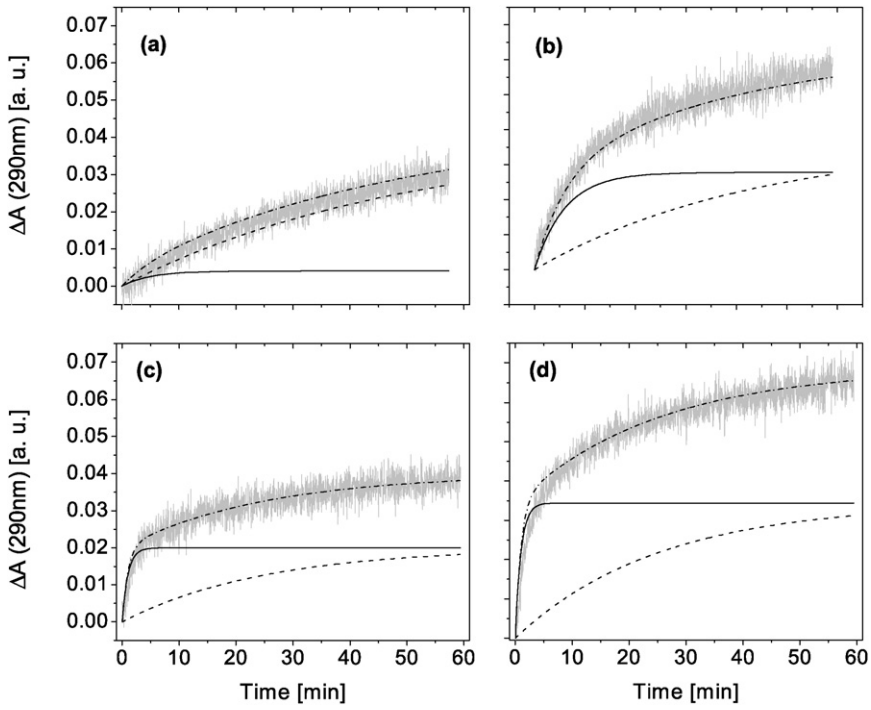

Fig. 9. Increase of absorbance during N_2O decomposition at 473 K (a, c) and 523 K (b, d) as a function of time at 290 nm after prereduction in 20% H_2/Ar. Temperature of prereduction: 673 K (a, b) and 873 K (c, d).

Table 1
Rate constants (k_1 and k_2) and differences of absorbance between $t = 0$ and 60 min for the fits of the reoxidation kinetics followed by in situ UV–vis-DRS (Fig. 9)

	Pretreatment				
	H_2/Ar, 673 K		H_2/Ar, 873 K		Ar, 873 K
T_{reox} (K)	473	523	473	523	523
Band maximum position 290 nm					
k_1 (min^{-1})	0.18	0.15	0.63	0.50	1.22
Δabs_1 (%)[a]	9.3	43.3	50.0	49.7	75.1
k_2 (min^{-1})	0.02	0.02	0.04	0.04	0.04
Δabs_2 (%)[a]	90.7	43.3	50.0	50.3	24.9
Band maximum position 234 nm					
k_1 (min^{-1})	0.55	0.26	0.59	0.84	1.60
Δabs_1 (%)[a]	21.9	40.4	52.7	56.2	75.6
k_2 (min^{-1})	0.02	0.02	0.04	0.04	0.04
Δabs_1 (%)[a]	78.1	59.6	47.3	43.8	24.4

[a] With respect to the total difference of absorbance before and after reductive pretreatment.

law [Eq. (2)] are plotted in Fig. 9, and the rate constants are summarized in Table 1. Satisfactory fits could be obtained only by assuming two different reoxidation processes, a fast process (site Fe1) and a slow one (site Fe2). Considering the in situ EPR study (Fig. 8), it seems probable that site Fe1 gives rise to the low-field signals at $g' = 6.4$, 5.6, and 4.3. They are saturated at 573 K, while the signal at $g' \approx 2$ grows further, suggesting that it arises preferentially from site Fe2 with the slower reoxidation rate. The absorbance difference at $t = 0$ and 60 min (Table 1) can be considered a measure for the relative percentage of each Fe site with respect to the total number of active sites. The higher pretreatment temperature of 873 K clearly favors the amount of the rapidly reoxidized site Fe1. Moreover, its formation rate (decomposition rate of N_2O) increases with rising pretreatment temperature (Table 1). On the other hand, the behavior of the slowly reoxidized site Fe2 is very similar for all conditions studied.

It is known from previous studies that high-temperature pretreatment in inert gas is also an efficient way to create highly active sites for abstracting O from N_2O [11,17,20]. Moreover, it was observed that such treatment is able to redisperse Fe_xO_y clusters and to enhance N_2O decomposition activity [39–44]. Therefore, in an analogous experiment pretreatment at 973 K was done in pure Ar instead of the H_2/Ar mixture. In this case, both the reoxidation rate and the amount of the highly active sites Fe1 were markedly higher than after pretreatment in H_2/He at the same temperature (Table 1). We postulate that pretreatment in Ar may have suppressed the clustering of highly active single Fe sites, an undesired effect occurring partially during pretreatment in H_2/Ar (Figs. 1b–1d). This is also suggested by comparing UV–vis spectra after N_2O decomposition at 523 K after pretreatment in H_2/Ar or pure Ar, respectively. In the latter case, absorbance above 350 nm (i.e., in the range of CT transitions of Fe_xO_y clusters), was lower than in the case of H_2/Ar pretreatment (not shown).

3.5. State of oxygen and Fe sites after deposition of oxygen from N_2O

In this section, we rely mainly on XANES and EPR data, because of all the methods used in this study, only XANES is sensitive to Fe oxidation states beyond +3 [29,42,43], whereas EPR is the only method capable of detecting candidate oxygen species in our context. XANES spectra measured after reoxida-

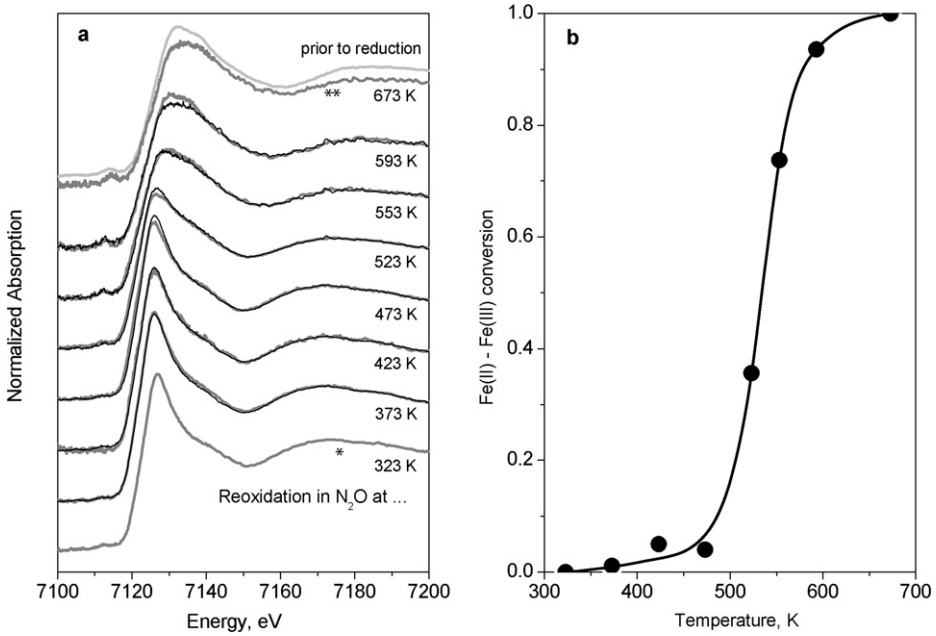

Fig. 10. (a) XANES spectra obtained after reoxidation of Fe-ZSM-5 by 2% N_2O/N_2 for 10 min at different temperatures: grey lines—experimental spectra, thin black lines—XANES fits obtained by superimposing two spectra being characteristic for Fe^{2+} (∗, identical with dashed spectrum in Fig. 2) and Fe^{3+} (∗∗). The reduced state was obtained by treatment of calcined Fe-ZSM-5 in 20% H_2/He at 810 K (cf. Fig. 2, reduction run I). (b) Development of reoxidation degree with temperature derived from XANES fits.

tion of the reduced Fe-ZSM-5 (cf. Fig. 2, run I) in flowing 2% N_2O/N_2 at different temperatures are shown in Fig. 10 (grey lines). At low temperatures, there is not much change of the spectral shape, but between 470 and 570 K, the absorption edge shifts, and the shape approaches that of the oxidized state. The spectrum measured after reoxidation at 673 K (denoted by ∗∗) is almost identical to that of the initial oxidized sample. The minor differences may be ascribed to clustering tendencies in the redox cycle as detected by UV–vis spectroscopy (Figs. 1b–1d). A principal component analysis (PCA) of the spectra after reoxidation at 373–593 K found four principal components, decreasing to two after omitting just one spectrum (523 K) [44]. Target transformation showed the spectrum after reoxidation at 323 K (∗) to be a principal component, the deviation for spectrum ∗∗ was small; that is, the (not exactly known) second component spectrum most likely belongs to a Fe^{3+} state as well. Hence, whereas reoxidation at all temperatures resulted only in Fe^{3+}, additional species may have been formed at 523 K. To explore their importance, the spectra of samples reoxidized at intermediate temperatures were fitted as linear combination of spectra denoted by ∗ (representing Fe^{2+}) and by ∗∗ (representing Fe^{3+}). The fits are on the whole very good (Fig. 10a, thin black curves), with noticeable deviations occurring after reoxidation at 593 K rather than 523 K. This suggests that also at 523 K, most of the Fe species are either Fe^{2+} or Fe^{3+}. The $Fe^{2+} \rightarrow Fe^{3+}$ reoxidation degrees derived from these fits are reported in Fig. 10b. The oxidation rate becomes significant only above 470 K, and the conversion is around 50% at 520–530 K, as observed earlier with UV–vis spectroscopy.

Thus, our XANES spectra provide strong evidence for the absence of Fe^{n+} ($n > 3$), although we had no access to reference materials with iron in higher oxidation states. Significant differences between Fe^{3+} and Fe^{4+} edge positions have been reported in the literature [29,42,43], including a 1.4-eV shift between Fe_2O_3 and the mixed Fe^{3+}/Fe^{4+} compound $SrFeO_{2.85}$ [42]. However, our XANES analysis, according to which the experimental spectra of partially reoxidized Fe-ZSM-5 are reproduced by a linear combination of subspectra from Fe^{2+} and Fe^{3+} species with resulting oxidation degrees in agreement with UV–vis data, allows us to rule out iron in higher oxidation states in any significant amount.

The combined data from the XANES, transient pulse, UV–vis, and EPR experiments suggest that N_2O decomposition at 523 K proceeds to a large extent on isolated Fe sites and without O_2 desorption. This finding is in agreement with previous studies of N_2O decomposition over Fe-MFI catalysts [19] and with recent DFT calculations [45,46]. As discussed above, this means that the ratio of deposited O and reoxidized Fe should roughly be equal to unity. According to Panov et al. [12], this would mean that the active species is a $Fe^{3+}O^{\cdot-}$ site. Because EPR spectroscopy is very sensitive for species containing unpaired electrons ($Fe^{3+}O^{\cdot-}$), we performed an EPR study of the first step (deposition of oxygen species without formation of gas-phase O_2) of N_2O decomposition over Fe-ZSM-5 that had been pretreated in Ar flow at 973 K for 1.5 h. Such pretreatment is essential for creating active Fe sites for N_2O decomposition, as demonstrated by our own UV–vis tests and by other authors [11,17,20]. After this treatment, marked autoreduction of Fe^{3+} is evident from Fig. 11 (spectrum 2) from the decreased signal intensity. The small remaining features in the middle field range (Fig. 11b) arise from the hyperfine structure signal of an V^{4+} impurity apparently introduced into the sample by the Fe powder used for the preparation (although a vanadium impurity is not mentioned in the manufacturer's specifications; see

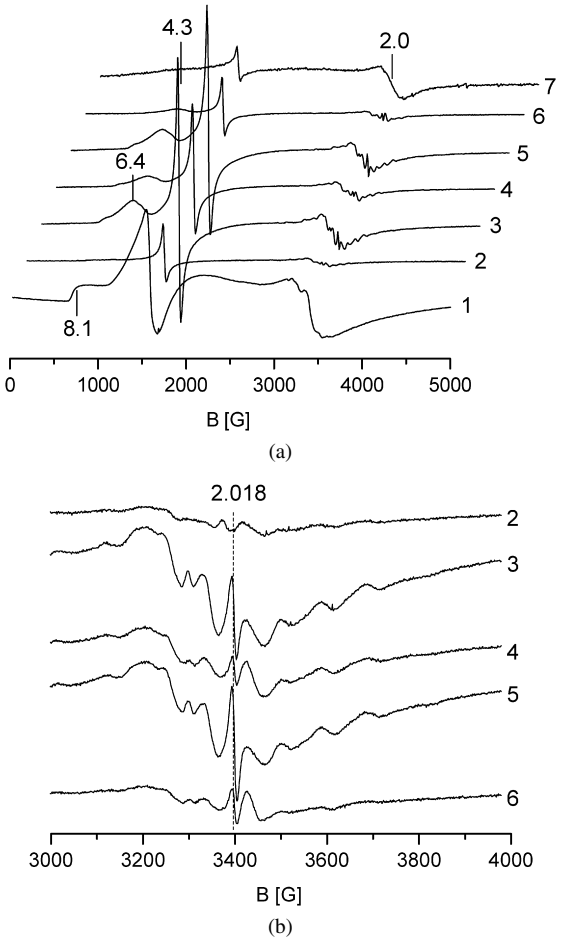

Fig. 11. EPR spectra measured at 77 K after the following sequential treatment (b) shows the enlarged middle field range of (a): (1) as-received, (2) 1.5 h in Ar flow at 973 K, (3) 30 min in 2% N_2O/He flow at 523 K, (4) 30 min in 5% CO/He flow at 293 K, (5) 30 min in 2% N_2O/He flow at 523 K, (6) 30 min in a 5% CO/He flow at 523 K, (7) 30 min in O_2 flow at 523 K and evacuation at 77 K.

also [1]). After exposure to N_2O, the signal at $g' \approx 4.3$ increases strongly and a new line at $g' \approx 6.4$ appears, suggesting that these particular isolated Fe^{3+} sites are formed when N_2O deposits its oxygen on Fe^{2+} species, as was found in the in situ experiments at reaction temperature (Fig. 8). A minor signal is also observed at $g' \approx 2$, suggesting that there may be a third kind of Fe species that can take up this oxygen. But whether this signal arises from highly symmetric isolated Fe sites or from small FeO_x clusters is difficult to determine. Nevertheless, this is clear evidence that isolated Fe sites are active ones; that is, the frequently discussed binuclear complex [11,12,15,23,47] is not necessary to form the active O species from N_2O, although their presence in the sample and similar reactivity are not excluded. Moreover, the spectra in Fig. 11 confirm in agreement with the XANES results (Fig. 10) that reduced Fe^{2+} is oxidized to Fe^{3+} and not to Fe^{4+}, which would not be visible at 77 K.

When an isolated Fe^{2+} takes up one oxygen to form Fe^{3+}, the oxygen atom must be $O^{\bullet-}$ and should be seen in the EPR spectrum. Indeed, we observe a radical signal at $g = 2.018$ (Fig. 11b, spectrum 3). It is superimposed on the hyperfine structure signal of the VO^{2+} impurity, which also is more pronounced after N_2O treatment. This impurity possibly may be reduced to EPR-silent V^{3+} during Ar treatment and reoxidized by N_2O as well. However, the shape of the observed radical signal is not typical for $O^{\bullet-}$, because the thermal motion of an $O^{\bullet-}$ species should be widely restricted at 77 K, and the typical axial EPR signal with $g_{\|} \approx g_e$ and $g_{\perp} > g_e$ [48] should be observed. This is not the case in Fig. 11b; instead, an isotropic radical line is detected at a g value of 2.018. The reason for this is discussed below, taking into account the results of microkinetic evaluation of N_2O decomposition under transient conditions [34,35] and DFT calculations [45,46]. Both approaches conclude that N_2O decomposes over reduced Fe sites

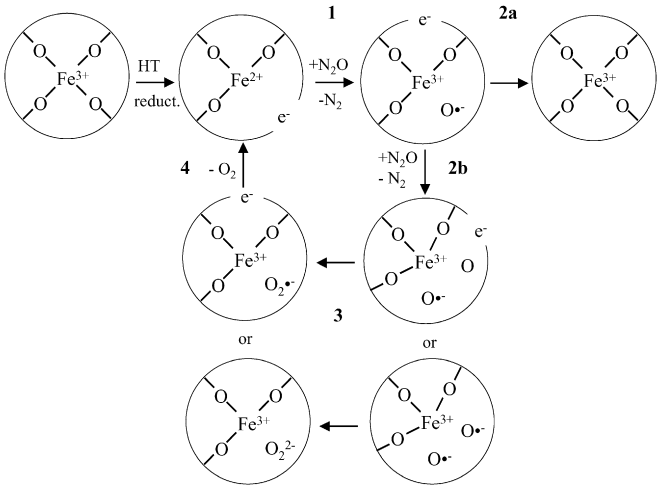

Fig. 12. Possible reaction scheme of N_2O decomposition on isolated Fe sites in Fe-ZSM, taking into account spectroscopic results of this work as well as the previously derived kinetic model (steps 1–4, Eqs. (3)–(6) [34,35]).

$$N_2O + * \rightarrow *\text{–}O + N_2, \tag{3}$$

and form Fe sites with deposited oxygen species, yielding a biatomic oxygen species

$$N_2O + *\text{–}O \rightarrow O\text{–}*\text{–}O + N_2. \tag{4}$$

However, the approaches differ in the reaction pathways of formation of gas-phase oxygen. The transient kinetics in [34,35] predict that O_2 formation occurs via reactions

$$O\text{–}*\text{–}O \rightarrow *\text{–}O_2, \tag{5}$$

$$*\text{–}O_2 \rightarrow O_2 + *, \tag{6}$$

whereas DFT calculations [45,46] assume that gas-phase O_2 is formed via the reaction

$$N_2O + *\text{–}O_2 \rightarrow *\text{–}O + N_2 + O_2. \tag{7}$$

Here $*$ represents an active iron species.

Because our EPR tests were performed under conditions in which O_2 was not formed, in what follows we consider the reaction steps in Eqs. (3)–(5) only. According to Kondratenko and Pérez-Ramírez [35], the dominating surface species below 600 K is O–*–O, with negligible surface concentrations of *–O and *–O_2; that is, reaction (4) is very fast, and reaction (5) virtually does not occur under these conditions. This is in agreement with the N_2O pulse experiments in this work demonstrating that

N_2O conversion at 523 K stops after saturation of active sites by deposited oxygen species (Fig. 4). According to the EPR results in Fig. 11b, the moiety O–∗–O in Eqs. (4) and (5) should comprise $O^{\bullet-}$ species. The close neighborhood of such oxygen radicals within the O–∗–O intermediate might result in dipolar and/or spin–spin exchange interaction between these oxygen species. Such interaction can average out g-tensor splittings, so the typical axial EPR signal with $g_{\|} \approx g_e$ and $g_{\perp} > g_e$ [48] is not observed. Instead, an isotropic radical line is detected at a g value of 2.018.

Further experimental evidence for the presence of $O^{\bullet-}$ species is provided by EPR measurements of the reactivity of this species with CO (Fig. 11). Panov and others [12,15,20] have found that O species deposited by N_2O are very reactive and hence oxidize CO at room temperature. We proved this by passing a flow of 5% CO/He at room temperature over the Fe-ZSM-5 catalysts, on which reactive oxygen species had been deposited by N_2O at 523 K. Comparison of Fe^{3+} EPR signals in N_2O-treated Fe-ZSM-5 (Fig. 11, spectrum 3) followed by CO treatment (Fig. 11, spectrum 4) shows that the intensity of both the Fe^{3+} signals and the radical signal decrease markedly on contact with CO. This suggests that both signals belong to the same single site, namely $Fe^{3+}O^{\bullet-}$. This behavior is completely reversible by retreating the sample at 523 K in N_2O flow (Fig. 11, spectrum 5). Subsequent treatment in CO at 523 K for 30 min leads to an even stronger decrease of the Fe^{3+} and the radical signal (Fig. 11, spectrum 6).

To prove whether the oxygen radical signal in Fig. 11 (spectrum 3) appears on interaction of Fe^{2+} species with O_2, after CO treatment at 523 K, the gas flow was switched to O_2 and held for 30 min at this temperature. Afterwards, the treated sample was rapidly quenched to 77 K and evacuated at this temperature, to prevent magnetic interaction of gaseous O_2 with exposed paramagnetic species. Interestingly, no Fe signal at $g' \approx 6.4$, no increase of the $g' \approx 4.3$, and no radical signal at $g' = 2.018$ can be seen (Fig. 11, spectrum 7). The VO^{2+} hfs structure also disappeared, most likely due to oxidation to diamagnetic VO^{3+}.

The results of these experiments clearly indicate that the activation of N_2O proceeds on single Fe sites and most likely leads to highly active $Fe^{3+}O^{\bullet-}$ species for which direct experimental evidence is obtained from EPR spectra. The possibility that the VO^{2+} impurity plays the same game cannot be fully excluded. However, because the unique oxidation properties have been observed only for Fe-ZSM-5 and not for V-ZSM-5, it is obvious that the major contribution comes from Fe, not from the VO^{2+} impurity.

Equation (4) implies that two oxygen species should be deposited for each reduced Fe site (represented by ∗), leading to a ratio of $O_{dep}/Fe_{active} = 2$. This is not in line with the above-discussed UV–vis and N_2O pulse experiments. A possible explanation for this apparent disagreement is provided by the reaction scheme in Fig. 12, in which isolated tetrahedrally coordinated Fe^{3+} inside a pore is considered as active site; however, the processes on an isolated higher-coordinated Fe site should be analogous. It is assumed that during reductive pretreatment at high temperature, an oxygen atom is removed by homolytic scission of the Fe^{3+}–O–support bond from the Fe coordination shell, leaving behind a reduced Fe^{2+} and, consequently, an additional electron that may be located in an anion vacancy. As suggested by in situ UV–vis and EPR studies, an $O^{\bullet-}$ anion radical is formed on reoxidation of such (activated) Fe^{2+} to Fe^{3+} with N_2O [Eq. (3)] but not with O_2. The resulting $Fe^{3+}O^{\bullet-}$ species has two reaction channels: (1) It can capture a free electron to regenerate the initial $Fe^{3+}O_4$ species, which is no longer active for N_2O decomposition (Fig. 12, step 2a), or (2) it can abstract a further O atom from a second N_2O molecule yielding the O–∗–O intermediate postulated in Eq. (4) (Fig. 12, step 2b). The latter then must be considered a $O^0(Fe^{3+})O^{\bullet-}$ species [or a $O^{\bullet-}(Fe^{3+})O^{\bullet-}$ species, in the event of capturing a free electron], which gives rise to the EPR radical signal in Fig. 11b. As shown by the kinetic model of Kondratenko and Pérez-Ramírez [35], step 3 in the scheme of Fig. 12 [Eq. (5)] virtually does not occur at temperatures as low as 598 K and $p_{N_2O} \leqslant 2$ kPa. Thus, an $O_2^{\bullet-}$ species as postulated after step 3 in Fig. 12 can be excluded as source of the radical signal in Fig. 11b, because the reaction temperature was only 523 K.

As discussed above, the comparison of N_2O pulse and UV–vis results suggests an $O_{dep}/Fe_{active} \approx 1$ ratio, in contradiction to the kinetic model, which suggests $O_{dep}/Fe_{active} \approx 2$. The reason for this discrepancy becomes obvious from inspecting Fig. 12. UV–vis spectroscopy detects not only the Fe^{3+} species involved in the formation of the O^0 $(Fe^{3+})O^{\bullet-}$ or $O^{\bullet-}(Fe^{3+})O^{\bullet-}$ intermediates (accounting for $O_{dep}/Fe_{active} \approx 2$), but also $Fe^{3+}O_4$ species formed from the $O_3Fe^{3+}O^{\bullet-}$ intermediate by electron capture, which thus become inactive for further N_2O decomposition. Thus, more Fe^{3+} than involved in the active catalytic cycle is detected. Further experimental evidence for the deactivation of initially active O species deposited by N_2O decomposition was recently obtained by sequentially pulsing N_2O and propane onto Fe-ZSM-5 and Fe-silicalite with an Fe content of 0.7 wt%; it was found that both methane and propane conversion decreased with the time delay between the N_2O and the subsequent hydrocarbon pulse [49].

4. Conclusions

Complementary transient pulse experiments and in situ studies by UV–vis DRS have shown that reduction in H_2/Ar or autoreduction in Ar at high temperatures creates highly active Fe^{2+} sites next to oxygen vacancies, which catalyze N_2O decomposition at 480–523 K without O_2 liberation. The vacancies are filled by atomic oxygen abstracted from N_2O, which reoxidizes Fe^{2+} to form Fe^{3+} and $O^{\bullet-}$ radical anions. For the first time, a direct relationship between the formation of both species could be detected by EPR spectroscopy, suggesting that the so-called "α-oxygen" first discovered by Panov et al. is an $O^{\bullet-}$ radical anion. Together with in situ XANES experiments, this makes it highly unlikely that the formation of a previously discussed ferryl moiety (Fe^{4+}=O) is a source of the highly active oxygen. It is clearly shown, that $O^{\bullet-}$ species form on electron transfer from isolated Fe sites, which, in their trivalent form, contribute to the EPR signals at $g' \approx 6.4, 5.6$, and 4.3. But the same process also may occur on small oligonuclear

Fe_xO_y clusters, as evidenced by changes in UV–vis CT bands above 300 nm and the EPR signal at $g' \approx 2$ during treatment in N_2O/He. In contrast to N_2O, no formation of $O^{\bullet-}$ could be observed on reoxidation with O_2.

Kinetic analysis of the Fe^{2+} reoxidation by in situ UV–vis DRS revealed two processes with different rates, a fast process and a slow process. The higher the prereduction temperature, T_{red}, the more abundant are the Fe sites involved in the fast process, whereas the number of slowly reoxidized Fe sites is almost independent on T_{red}. This suggests that the rapidly reoxidized Fe sites are not easily reduced, whereas the opposite is true for the slowly reoxidized ones. Comparison with EPR results shows that isolated Fe^{3+} sites in both tetrahedral ($g' \approx 4.3$) and higher coordination ($g' \approx 6.4, 5.6$) form during the fast process, whereas small oligonuclear $Fe_x^{3+}O_y$ clusters ($g' \approx 2$) are created slowly from the respective reduced Fe sites. Considering the results of Wichterlová and co-workers [36–38], who identified different sites for isolated metal ions in ZSM-5 in the straight channels (α), in the intersection between the straight and sinusoidal channels (β), and in a boat-shaped site in the sinusoidal channel (γ), all of which have differing sensitivities against reduction, it seems plausible to relate the low-field EPR signals, based on their redox behavior, to Fe^{3+} sites in β ($g' \approx 6.4$ and 5.6) and γ sites ($g' \approx 4.3$) and the EPR line at $g' \approx 2$ line to isolated sites in α sites as well as to small clusters in the main channels of the ZSM-5 structure.

Acknowledgments

This work was supported by the German Science Foundation (grants BR 1380/11-2 and Gr 1447/7).

References

[1] M. Schwidder, M. Santhosh Kumar, K. Klementiev, M.-M. Pohl, A. Brückner, W. Grünert, J. Catal. 231 (2005) 314.
[2] X. Feng, W.K. Hall, Catal. Lett. 41 (1996) 45.
[3] H.-Y. Chen, W.M.H. Sachtler, Catal. Today 42 (1998) 73.
[4] G.I. Panov, G.A. Sheveleva, A.S. Kharitonov, V.N. Romannikov, L.A. Vostrikova, Appl. Catal. A Gen. 82 (1992) 31.
[5] A. Ribera, I.W.C.E. Arends, S. de Vries, J. Perez-Ramirez, R. Sheldon, J. Catal. 195 (2000) 287.
[6] E.J.M. Hensen, Q. Zhu, R.A.J. Janssen, P.C.M.M. Magusin, P.J. Kooyman, R.A. van Santen, J. Catal. 233 (2005) 123.
[7] J.F. Jia, K.S. Pillai, W.M.H. Sachtler, J. Catal. 221 (2004) 119.
[8] E. Kondratenko, J. Pérez-Ramírez, Appl. Catal. A Gen. 267 (2004) 181.
[9] B.R. Wood, J.A. Reimer, A.T. Bell, M.T. Jannicke, K.C. Ott, J. Catal. 224 (2004) 148.
[10] M. Santhosh Kumar, J. Pérez-Ramírez, M.N. Debbagh, B. Smarsly, A. Brückner, Appl. Catal. B Environ. 62 (2006) 244.
[11] K.A. Dubkov, N.S. Ovanesyan, A.A. Shteinman, E.V. Starokon, G.I. Panov, J. Catal. 207 (2002) 341.
[12] G.I. Panov, A.K. Uriate, M.A. Rodkin, V.I. Sobolev, Catal. Today 41 (1998) 365.
[13] E.V. Starokon, K.A. Dubkov, L.V. Pirutko, G.I. Panov, Top. Catal. 23 (2003) 137.
[14] J. Pérez-Ramírez, M. Santhosh Kumar, A. Brückner, J. Catal. 223 (2004) 13.
[15] L. Kiwi-Minsker, D.A. Bulushev, A. Renken, J. Catal. 219 (2003) 273.
[16] A.L. Yakovlev, G.M. Zhidomirov, Catal. Lett. 63 (1999) 91.
[17] D.A. Bulushev, L. Kiwi-Minsker, A. Renken, J. Catal. 222 (2004) 389.
[18] J. Jia, Q. Sun, B. Wen, L.X. Chen, W.M.H. Sachtler, Catal. Lett. 82 (2002) 7.
[19] G. Pirngruber, J.-D. Grunwaldt, P. Roj, J. van Bokhoven, O. Safonova, P. Glatzel, Second International Congress on Operando Spectroscopy, April 23–27, 2006, Toledo, Spain, Book of Abstracts, p. 128.
[20] J. Nováková, M. Schwarze, Z. Tvarůžková, Z. Sobalik, Catal. Lett. 98 (2004) 123.
[21] F.W.H. Kampers, T.M.J. Maas, J. van Grondelle, D.C. Brinkgreve, D.C. Koningsberger, Rev. Sci. Instrum. 60 (1989) 2635.
[22] XANES dactyloscope for Windows, freeware http://www.desy.de/~klmn/xanda.html.
[23] M. Santhosh Kumar, M. Schwidder, W. Grünert, A. Brückner, J. Catal. 227 (2004) 384.
[24] J. Pérez-Ramirez, J.C. Groen, A. Brückner, M. Santhosh Kumar, U. Bentrup, M.N. Debbagh, L.A. Villaescusa, J. Catal. 232 (2005) 318.
[25] S. Bordiga, R. Buzzoni, F. Geobaldo, C. Lamberti, E. Giamello, A. Zecchina, G. Leofanti, G. Petrini, G. Tozzolo, G. Vlaic, J. Catal. 158 (1996) 486.
[26] G. Lehmann, Z. Phys. Chem. Neue Folge 72 (1970) 279.
[27] G.A. Waychunas, M.J. Apted, G.E. Brown Jr., Phys. Chem. Miner. 10 (1983) 1.
[28] W.M. Kwiatek, M. Galka, A.L. Hanson, C. Paluszkiewicz, T.J. Cichicki, Alloys Comp. 328 (2001) 276.
[29] G.M. Veith, I.D. Fawcett, M. Greenblatt, M. Croft, I. Nowik, Int. J. Inorg. Mater. 2 (2000) 513.
[30] R.W. Joyner, M. Stockenhuber, Catal. Lett. 45 (1998) 15.
[31] K. Inamura, R. Iwamoto, A. Iino, T. Takyu, J. Catal. 142 (1993) 273.
[32] F. Heinrich, C. Schmidt, E. Löffler, M. Menzel, W. Grünert, J. Catal. 212 (2002) 157.
[33] E.M. El-Malki, R.A. van Santen, W.M. Sachtler, J. Catal. 196 (2000) 212.
[34] E.V. Kondratenko, J. Pérez-Ramírez, J. Phys. Chem. B 110 (2006) 22586.
[35] E.V. Kondratenko, J. Pérez-Ramírez, Catal. Today 121 (2007) 197.
[36] J. Dědeček, D. Kaucky, B. Wichterlová, Microporous Mesoporous Mater. 35–36 (2000) 483.
[37] L. Čapek, V. Kreibich, J. Dědeček, T. Grygar, B. Wichterlová, Z. Sobalík, J.A. Martens, R. Brosius, V. Tokarová, Microporous Mesoporous Mater. 80 (2005) 279.
[38] B. Wichterlová, J. Dědeček, Z. Sobalík, Proceedings of the 12th International Zeolite Conference, vol. II, Mater. Res. Soc., Warrendale, PA, 1999, p. 941.
[39] Q. Zhu, R.M. van Teeffelen, R.A. van Santen, E.J.M. Hensen, J. Catal. 221 (2004) 575.
[40] G.D. Pirngruber, P.K. Roy, N. Weiher, J. Phys. Chem. B 108 (2004) 13764.
[41] K. Krishna, M. Makkee, Catal. Lett. 106 (2006) 183.
[42] M. Allix, D. Pelloquin, F. Studer, N. Nguyen, A. Wahl, A. Maignan, B. Raveau, J. Solid State Chem. 167 (2002) 48.
[43] M. Holzapfel, O. Proux, P. Strobel, C. Darie, M. Borowski, M. Morcette, J. Mater. Chem. 14 (2004) 102.
[44] S.R. Wasserman, J. Phys. IV 7 (1997) C2.
[45] A. Heyden, F.J. Keil, B. Peters, A.T. Bell, J. Phys. Chem. B 109 (2005) 1857.
[46] A. Heyden, A.T. Bell, F.J. Keil, J. Catal. 233 (2005) 26.
[47] P. Marturano, L. Drozdova, A. Kogelbauer, R. Prins, J. Catal. 192 (2000) 236.
[48] M. Che, A.J. Tench, Adv. Catal. 31 (1982) 77.
[49] E.V. Kondratenko, J. Pérez-Ramírez, Appl. Catal. B 64 (2006) 35.